A conformal mapping technique to correlate the rotating flow around a wing section of vertical axis wind turbine and an equivalent linear flow around a static wing

2013 Environ. Res. Lett. 8 044040

(http://iopscience.iop.org/1748-9326/8/4/044040)

OPEN ACCESS
IOP PUBLISHING
ENVIRONMENTAL RESEARCH LETTERS
Environ. Res. Lett. **8** (2013) 044040 (10pp)
doi:10.1088/1748-9326/8/4/044040

A conformal mapping technique to correlate the rotating flow around a wing section of vertical axis wind turbine and an equivalent linear flow around a static wing

Hiromichi Akimoto[1], **Yutaka Hara**[2], **Takafumi Kawamura**[3], **Takuju Nakamura**[4] **and Yeon-Seung Lee**[1]

[1] Division of Ocean Systems Engineering, Korea Advanced Institute of Science and Technology, 291 Daehak-ro, Yuseong-gu, Daejeon 305-701, Republic of Korea
[2] Department of Mechanical and Aerospace Engineering, Tottori University, 4-101 Koyama, Minami, Tottori 680-8552, Japan
[3] Computational Fluid Dynamics Consulting Inc., 2-1-1 Namiki, Tokorozawa, Saitama 359-0042, Japan
[4] MODEC, Inc., 3-10, Nihonbashi 2-chome, Chuo-ku, Tokyo 103-0027, Japan

E-mail: akimoto@kaist.ac.kr

Received 8 August 2013
Accepted for publication 6 November 2013
Published 25 November 2013
Online at stacks.iop.org/ERL/8/044040

Abstract
In a vertical axis wind turbine (VAWT), turbine blades are subjected to the curved flow field caused by the revolution of turbine. However, performance prediction of VAWT is usually based on the fluid dynamic coefficients obtained in wind tunnel measurements of the two-dimensional static wing. The difference of fluid dynamic coefficients in the curved flow and straight flow deteriorates the accuracy of performance prediction. To find the correlation between the two conditions of curved and straight flow, the authors propose a conformal mapping method on complex plane. It provides bidirectional mapping between the two flow fields. For example, the flow around a symmetric wing in the curved flow is mapped to that around a curved (cambered) wing in the straight flow. Although the shape of mapped wing section is different from the original one, its aerodynamic coefficients show a good correlation to those of the original in the rotating condition. With the proposed method, we can reproduce the local flow field around a rotating blade from the flow data around the mapped static wing in the straight flow condition.

Keywords: conformal mapping, vertical axis wind turbine, marine current turbine, blade performance, virtual camber

1. Introduction

In a vertical axis wind turbine (VAWT), the flow field around a turbine blade shows more complexity than those in a horizontal axis wind turbine (HAWT). The ambient flow of a VAWT blade changes its relative direction to the blade periodically and stream lines of the flow have a curvature. Muraca *et al* [1] described the effect of curved flow as the longitudinal variation of effective attack angle on the flat plate wing. Migliore *et al* [2–4] stated the virtual camber effect caused by the curved flow as shown in figure 1. However, these results do not show quantitative evaluation of the effect

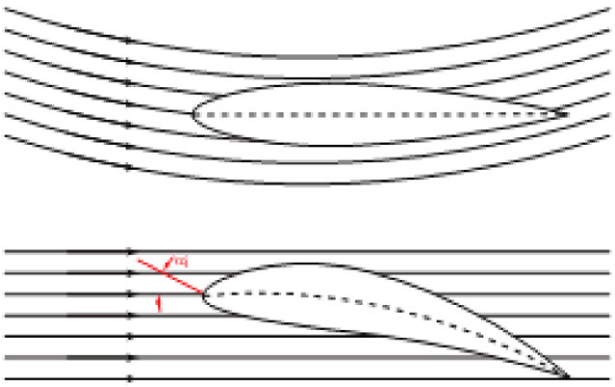

Figure 1. The principle of virtual camber as a result of curvilinear flow [2].

that is required to interpret the wind tunnel measurement of a two-dimensional (2D) wing to the condition of rotating VAWT blade.

Multiple-stream-tube [5] method and double multiple-stream-tube [6] method are popular tools for the performance prediction of VAWT. These methods depend on the aerodynamic coefficients of the 2D wing section mainly obtained in the straight flow of wind tunnels. Although there are experimental data of 2D wing sections [7, 8], the neglected effect of flow curvature deteriorates the accuracy of the performance prediction of VAWT especially in high solidity configurations. Although VAWT is not as popular as the HAWT in large-scale applications, recent researches show that there are possibilities of large-scale floating offshore VAWT concepts [9–12]. Because of the size of offshore wind project, we need more accurate performance prediction of VAWT. The applications of vertical axis marine current turbine [13, 14] also increase the importance of the prediction.

One solution of the problem is to find the method of correlation between curved and straight flows around the blade. Ågren *et al* [15] used a conformal mapping of the flow around a rotating blade to the flow around a cylinder to obtain the dynamic performance of VAWT in the potential theory. However, their conformal mapping does not take into account the curvature of ambient flow. Migliore and Wolfe [4] proposed a conformal mapping between curved and straight flow for the treatment of local attack angle. Since it is only a geometrical mapping using polar coordinates, the correlation between two flow fields is not clear. Furukawa *et al* [16] proposed a conformal mapping for explaining the effect of rotation on the performance of vertical axis water turbine. The discussion is on the transformation of flow distribution on the mean line of wing section. Takamatsu *et al* [17] derived the empirical formula to express the performance of a rotating water turbine blade using the aerodynamic characteristics of the wing obtained in wind tunnel measurements.

In the present paper, the authors propose a conformal mapping on a complex plane for the bidirectional interpretation between the straight rectilinear and curved flow fields. The main part of the mapping function is mathematically the same as that proposed by Furukawa *et al* [16]. The function will map the curved flow around the original wing section to the straight flow around a modified wing section with an additional camber. Although the mapped wing shape is different from the original one, the local flow around the wing preserves the main features of the curved flow condition.

2. Mapping of flow field

2.1. Geometric mapping

We consider a bidirectional mapping between two complex number planes shown in figure 2. The straight uniform flow on ζ-plane in figure 2(a) is mapped to the rotating curved flow on z-plane in figure 2(b). Complex numbers on ζ- and z-planes are denoted as $\zeta = \xi + \mathrm{i}\eta$ and $z = x + \mathrm{i}y$ respectively, using the imaginary unit i and real numbers ξ, η, x and y.

A simple mapping function $g_0(\zeta)$ in equation (1) maps the real axis of ζ-plane to the circle of radius R on z-plane which indicates the path of blade in a rotating VAWT.

$$z = g_0(\zeta) = g_0(\xi + \mathrm{i}\eta) = (R + \eta)\mathrm{e}^{-\frac{\mathrm{i}}{R}\xi}. \tag{1}$$

The components of ζ and z have the following relation,

$$x + \mathrm{i}y = g_0(\xi + \mathrm{i}\eta) = (R + \eta)\left(\cos\frac{\xi}{R} - \mathrm{i}\sin\frac{\xi}{R}\right). \tag{1'}$$

It will map the wing chord length c on the real axis in straight flow (ζ-plane) to the circular arc of radius R in the curved flow (z-plane). A symmetric wing section with zero angle of attack on ζ-plane will be mapped to the cambered wing as shown in figure 2. Since the wing chord on ζ-plane is mapped to the curved mean line of the wing on z-plane, the chord length of the mapped wing becomes $R\{1 - \cos(c/2R)\}$. It is slightly shorter than c in the order of $\frac{1}{2}(c/2R)^2$.

Although equation (1) maps the wing geometry, it is not useful for mapping a velocity potential. Since $g_0(\zeta)$ contains the complex conjugation to derive real and imaginary parts of η separately, it is not a regular function and the mapped flow field does not satisfy the condition of ideal flow.

2.2. Fluid dynamically consistent mapping

For mapping the velocity potential, the authors propose a regular function,

$$z = g_1(\zeta) = R\mathrm{e}^{-\frac{\mathrm{i}}{R}\zeta}. \tag{2}$$

The components in the map are,

$$\begin{aligned} x + \mathrm{i}y &= g_1(\xi + \mathrm{i}\eta) \\ &= R\mathrm{e}^{\frac{\eta}{R}}\left(\cos\frac{\xi}{R} - \mathrm{i}\sin\frac{\xi}{R}\right). \end{aligned} \tag{2'}$$

The new function also maps the real axis of ζ-plane to the circle of radius R on z-plane, i.e. $g_1(\xi) = g_0(\xi)$. If the flow on ζ-plane is ideal (potential flow), it will be mapped to another potential flow on z-plane with the additional curvature of flow. Equation (2′) is mathematically the same as the function proposed by Furukawa *et al* [16] for the deformation of mean line in their vertical axis water turbine blade.

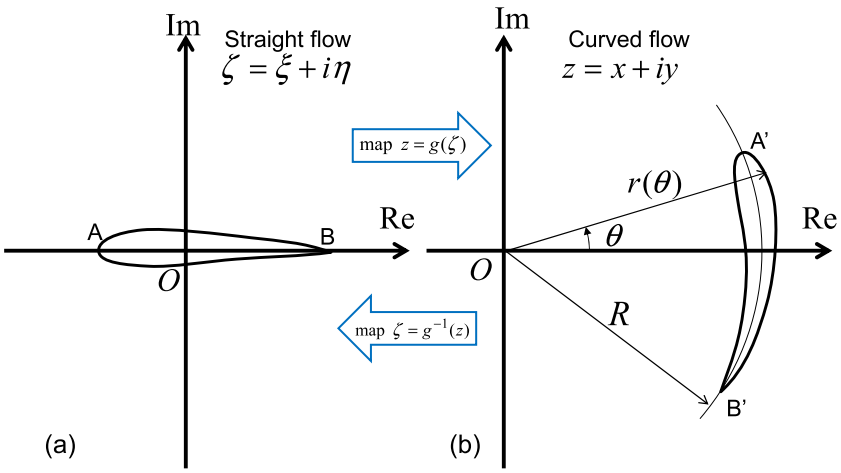

Figure 2. Geometric 2D mappings between (a) the straight rectilinear flow and (b) the rotating curved flow.

The complex velocity on z-plane is $q_c = d\phi(z)/dz$. Because the equivalent complex velocity potential on the straight flow is written as $\phi(z) = \phi(g_1(\zeta))$, the complex velocity q_s in the straight flow is,

$$q_s = \frac{d}{d\zeta}\phi(z) = \phi'(z)\frac{dz}{d\zeta} = \phi'(z)g_1'(\zeta) = q_c g_1'(\zeta). \quad (3)$$

The equation is applicable only to regular functions. Since the previous geometric map $g_0(\zeta)$ is not regular, the benefit of equation (3) is not available. The first derivative of $g_1(\zeta)$ is $g_1'(\zeta) = -ie^{-\frac{i}{R}\zeta}$ and its magnitude is $|g_1'(\zeta)| = e^{\frac{\eta}{R}}$. It indicates that the magnitude of mapped velocity will be modified according to the distance from the real axis. However, the difference is not significant in the typical thickness of wing section. For example, a wing of 20% thickness and rotating in the radius of $R = 5c$, the factor at the maximum thickness is $|g_1'(\zeta)| = e^{\pm 0.02}$. It gives 1.0202 and 0.9802 on the upper and lower surface respectively. The change of velocity is for keeping the condition of ideal flow and does not mean the error nor loss of information in the mapping process. The circulation around the wing is kept unchanged in the mapping.

The map $g_1(\varsigma)$ changes the thickness of wing section. The η coordinates of two points on the upper and lower surface of a wing with thickness t are $\eta = \pm t/2$. The distance between them is mapped to $t' = Re^{+t/2R} - Re^{-t/2R} = t + t^3/24R^2 + O(t^4)$. The change of thickness $t^3/24R^2$ is negligible. For example, the value for a wing of 20% thickness and rotating radius $R = 5c$ is $1.3 \times 10^{-5}c$.

2.3. Transformation of the fluid dynamically consistent map

For the practical use, it is convenient to add a rotational and translational operations to the present mapping function $g_1(\zeta)$ so that the mapped wing is near the origin and in the same orientation of the original as shown in figure 3. The modified regular function $g_2(\zeta)$ is,

$$z = g_2(\zeta) = e^{i\frac{\pi}{2}}g_1(\zeta) - iR = iRe^{-\frac{i}{R}\zeta} - iR. \quad (4)$$

The components of the map are,

$$x + iy = g_2(\xi + i\eta) = Re^{\frac{\eta}{R}}\sin\frac{\xi}{R} + iR\left(e^{\frac{\eta}{R}}\cos\frac{\xi}{R} - 1\right). \quad (4')$$

It will map the real axis on the rectilinear plane to the circular arc of radius R which passes through the origin ($z = 0$). The origin $\zeta = 0$ is the invariant point of the mapping. In the limit of $R \to \infty$, the map becomes the identity transformation.

2.4. Inverse mapping from rotating flow to rectilinear flow

The inverse map $g_1^{-1}(z)$ and its components are,

$$\varsigma = g_1^{-1}(z) = iR(\log z - \log R), \quad (5)$$

$$\xi + i\eta = g_1^{-1}(z) = -R\arg(x, y) + iR(\tfrac{1}{2}\log(x^2 + y^2) - \log R). \quad (5')$$

They map the circular arc on the curved flow to the real axis in the rectilinear flow in figure 2. The inverse map $g_2^{-1}(z)$ shown in figure 3 is,

$$\varsigma = g_2^{-1}(z) = iR\left(\log(z + iR) - \log R - i\frac{\pi}{2}\right), \quad (6)$$

$$\xi + i\eta = g_2^{-1}(z) = R\left(\frac{\pi}{2} - \arg(x, y + R)\right) + iR(\tfrac{1}{2}\log(x^2 + (y + R)^2) - \log R). \quad (6')$$

Here, the function $\arg(a, b)$ is the argument of $z = a + ib$. If a symmetric wing section is on ζ-plane with its midpoint chord at $\zeta = 0$ and without angle of attack, its mapped image on z-plane by $g_2(\zeta)$ has the camber height of $R\{1 - \cos(c/2R)\}$ in outward direction from the turbine axis. On the other hand, a symmetric wing in the curved flow on z-plane will be mapped to a reversed camber profile.

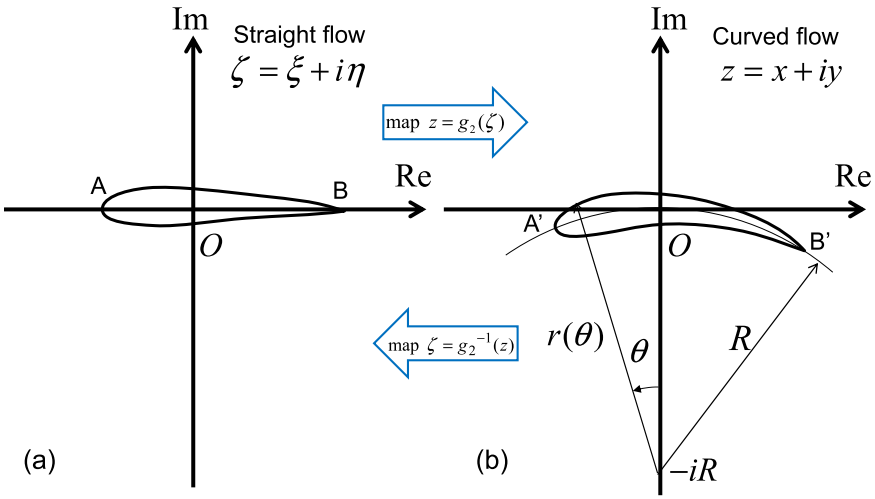

Figure 3. Conformal mapping between (a) the straight flow and (b) the curved flow with the adjustment of wing position.

2.5. Applications of the conformal mapping

The previous discussions are applicable only to ideal flow (potential flow). However, if the flow field around the turbine blade is dominated by potential flow, the proposed mapping will be a good approximation. It is true especially in the high Reynolds number flow and the wing is not in a stall condition. In the condition, the non-ideal flow region will be limited only in the thin boundary layer and trailing wake of the wing.

Since the experiment of rotating turbine is more expensive than that of the 2D static wing in a wind tunnel, effective utilization of the static measurement is highly beneficial to the R&D of VAWT. To take into consideration the flow curvature effect, we can prepare the wing section for the wind tunnel test using the mapping function described in section 2.4. Although the wing section is different from the original one, the regular conformal mapping reconstructs the local velocity field around the rotating blade from the static 2D result.

3. Numerical results and discussion

Because the present technique is based on the theory of ideal flow, the influence of viscosity and boundary layer to the correlation should be clarified. For this purpose, the authors conduct the computational fluid dynamics simulations around a wing in rotating and straight flow conditions with two Reynolds numbers.

3.1. Effective camber of the wing in curved flow

To simplify the problem, we consider a blade rotating around the turbine axis without incident uniform flow. It is equivalent to the high tip-speed-ratio condition. The flow is tested in the commercial Reynolds averaged Navier–Stokes (RaNS) solver ANSYS FLUENT 12.1. A sample of the computational mesh is shown in figure 4. In the present analysis, we consider the symmetric blade in the rotating flow and its mapped wing with camber in the straight flow. The situation often happens in the development of small VAWTs.

In the curved flow simulation, Coriolis force and the centrifugal force are added by the moving reference frame setting of FLUENT. The slot in the circular domain is to remove the cyclic effect caused by the wake of blade. The tested wing sections are NACA0018 and NACA0009 for the comparison of the effect of wing thickness. The radius of blade rotation is $R = 5c$. Tested Reynolds numbers are 3.6×10^5 and 3.6×10^6 based on the chord length and tangential speed at the blade. These two Reynolds numbers are for checking the influence of viscosity and the boundary layer thickness to the mapping. Turbulence model is the transition SST model. The angle of attack is 0 at the midpoint of the wing chord. The original wing sections are tested in the curved flow and their modified sections by the map $\zeta = g_2^{-1}(z)$ are tested in the straight flow.

Figure 5(a) shows the pressure contour around the rotating blade. The white line shows the curved path of the reference point (50%c). The leading and trailing edges are outer side of the curved path. Although the wing section is symmetric and without the angle of attack, it shows the asymmetric pressure distribution which exerts lift force inward to the rotating center.

Figure 5(b) shows the flow field around the modified wing mapped by $\varsigma = g_2^{-1}(z)$ in the straight flow. The mapped wing section has an inward camber of 2.50%c which imitates the effect of curved flow. The white line indicates the undisturbed straight flow passing through the reference point. The leading and trailing edges are not on the line. The RaNS simulation around the mapped wing is expected to reproduce the similar velocity field around the curved wing. The condition also provides the similar pressure distribution around the wing because of the Bernoulli's equation. However, the assumption is not applicable inside the velocity boundary layer because potential flow is not dominant there. On the rear lower wing surface in figure 5(b′), there are the separation and transition of turbulent boundary layer. It is not recognized in the curved flow condition as shown in figure 5(a′).

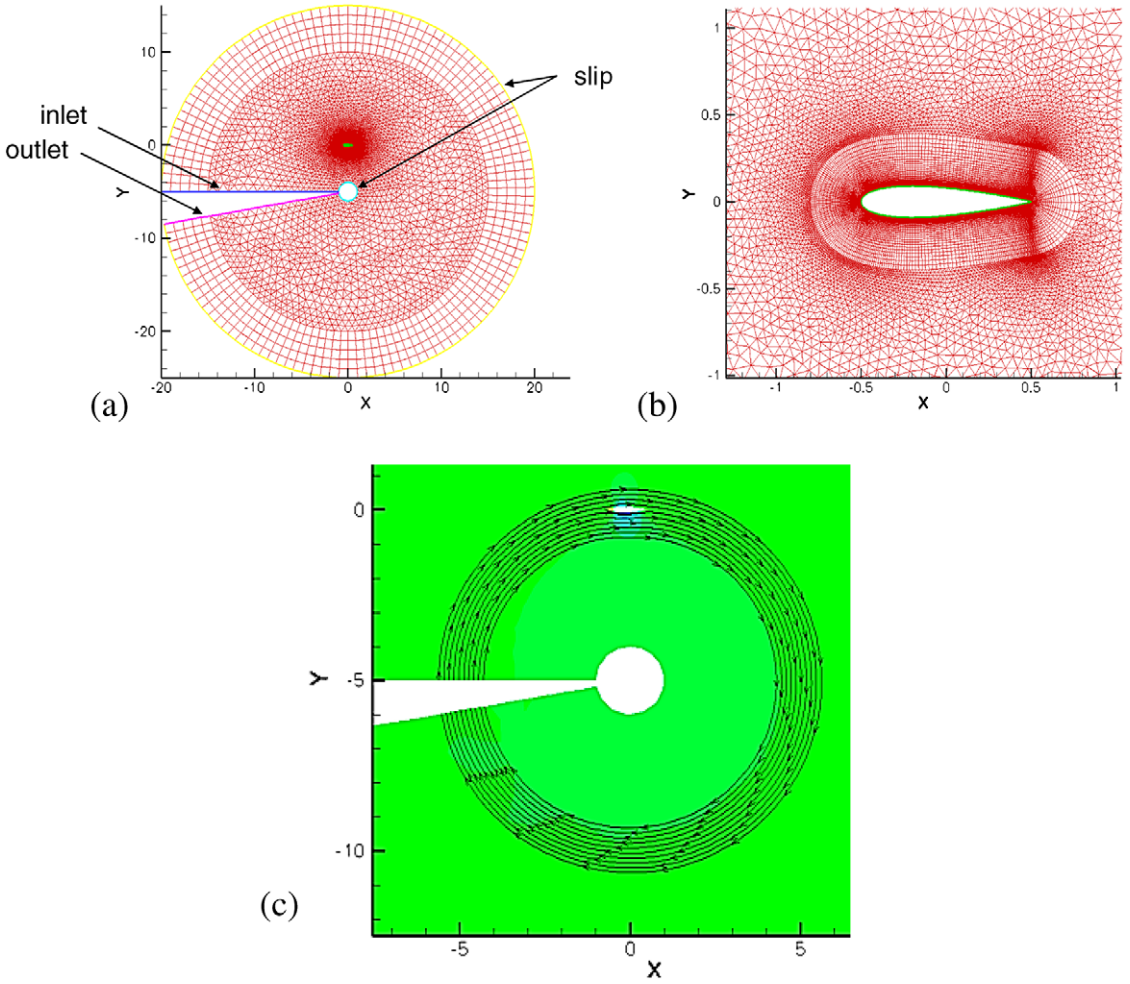

Figure 4. Computational mesh around the rotating blade; (a) overall domain, (b) close up view around the wing section and (c) stream lines in the computational domain.

Figure 6 shows the pressure distributions on the wing section. The pressure distribution on the rotating symmetry wing in figure 6(a) is reproduced by the RaNS simulation around the modified static wing section in figure 6(b). The difference in the rear part of figure 6(b) is caused by the boundary layer which can be seen in the previous picture of figures 5(b) and (b′). It indicates the difference in the transition of boundary layer between the curved and straight flow in the low Reynolds number ($Re = 3.6 \times 10^5$).

To compare the pressure distribution on the same geometry, the result in figure 6(b) is mapped to the original NACA0018 wing section and overset to the result of rotating blade as shown in figure 6(c). The agreement of the distribution is in a satisfactory level except the variation caused by the difference of boundary layer in the tail part. The discrepancy is reduced in the higher Reynolds number condition ($Re = 3.6 \times 10^6$) as shown in figure 6(d). In high Reynolds number conditions, viscous effect is significant only in the thin boundary layer and the correlation based on the regular complex number mapping is successful. However, the thick boundary layer or difference of boundary layer transition in a low Reynolds number condition deteriorates the accuracy of the proposed treatment.

Figure 7 shows the pressure contours around NACA0009 wing section as a sample of thin wing to check the influence of wing thickness to the mapping. Simulation conditions are as same as those of NACA0018 case and the Reynolds number is 3.6×10^6. Although the wing has neither a camber nor angle of attack, the curved flow provides asymmetric pressure field which indicates the lift force toward the rotational axis as shown in figure 7(a). The effect of flow curvature is replaced by the effect of camber on the mapped wing in figure 7(b).

The comparison of pressure distributions are shown in figure 8 in the same manner of figure 6. The overset comparison on the original wing in figure 8(c) shows that the agreement of two fields are in a satisfactory level and that the straight flow simulation of the mapped wing shape is equivalent to the rotating RaNS simulation.

Figure 9 shows the lift and drag coefficients in the variation of two wing sections (NACA0018 and NACA0009) and two Reynolds number conditions (3.6×10^5 and 3.6×10^6). The relative difference of lift coefficient between curved and straight flow is from 5 to 8%. The relative difference in the drag coefficients is higher than in the lift coefficients. However, the correlation of frictional drag which is the major part of drag has not been discussed yet. Since the pressure

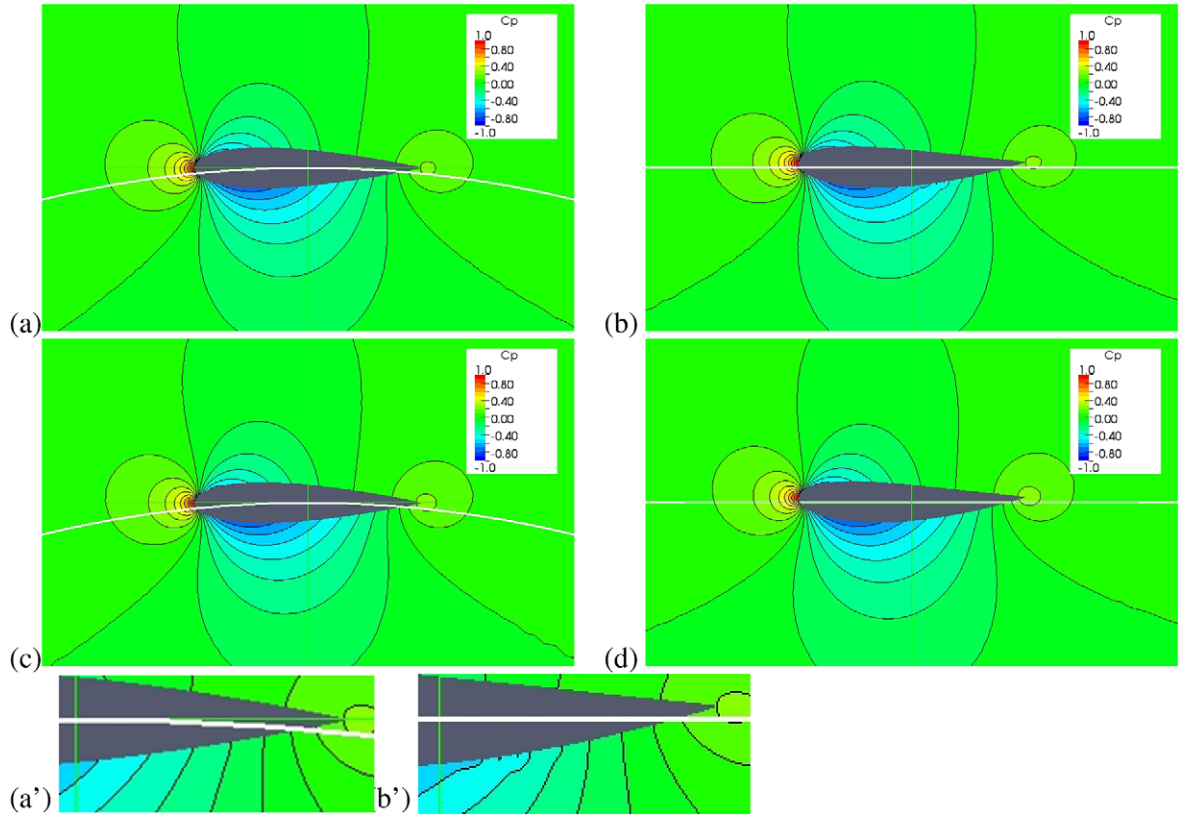

Figure 5. Pressure contour around the NACA0018 wing; (a) in curved flow and (b) the mapped wing in straight flow ($Re = 3.6 \times 10^5$); the high Reynolds number conditions of (c) curved and (b) straight flow ($Re = 3.6 \times 10^6$); (a′) and (b′) are close up views of the tail part of (a) and (b).

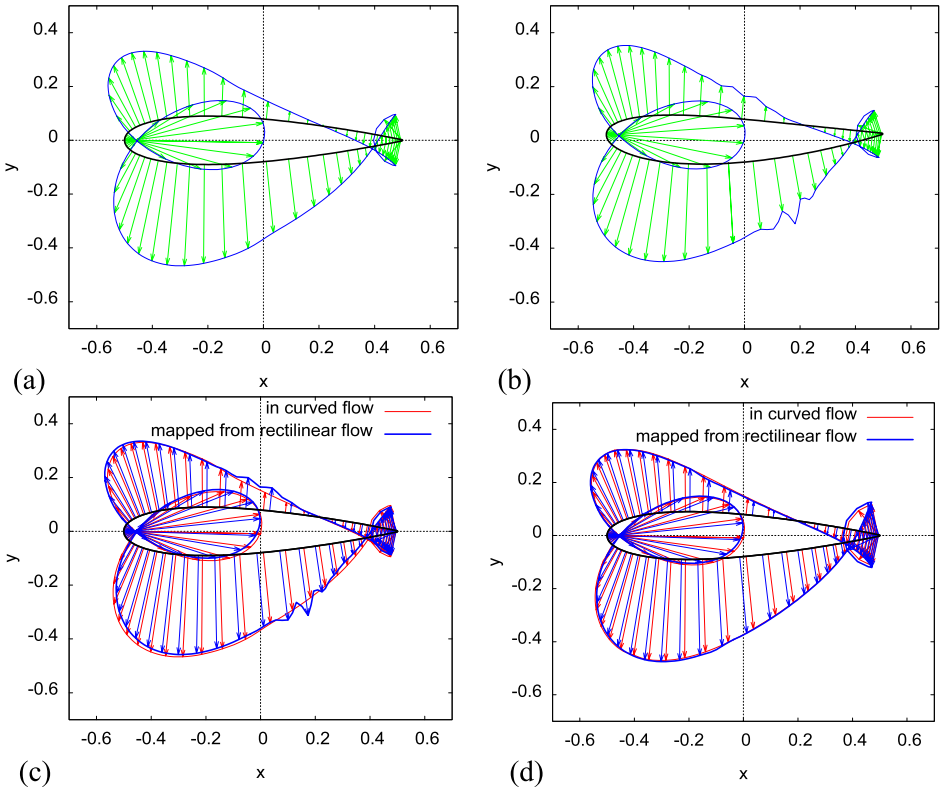

Figure 6. Pressure distributions on NACA0018 wing section; (a) in curved flow, (b) modified wing in straight flow and (c) comparison on the original wing section ($Re = 3.6 \times 10^5$); (d) comparison in higher Reynolds number ($Re = 3.6 \times 10^6$).

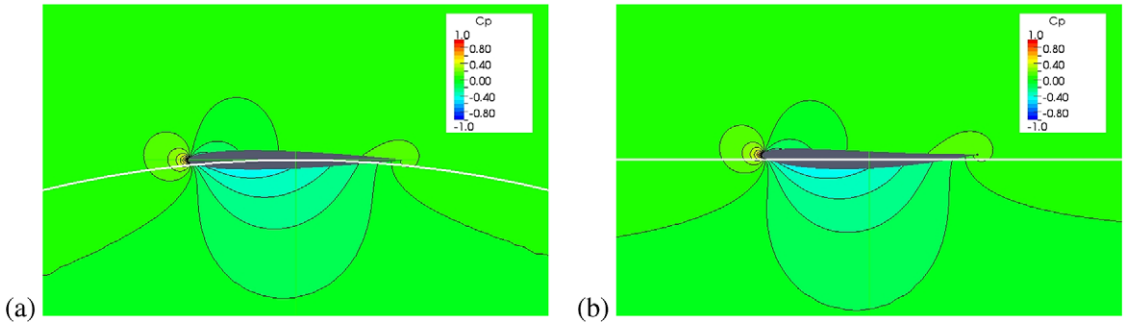

Figure 7. Pressure contour around NACA0009 wing section; (a) original section in curved flow and (b) mapped wing section in straight flow ($Re = 3.6 \times 10^6$).

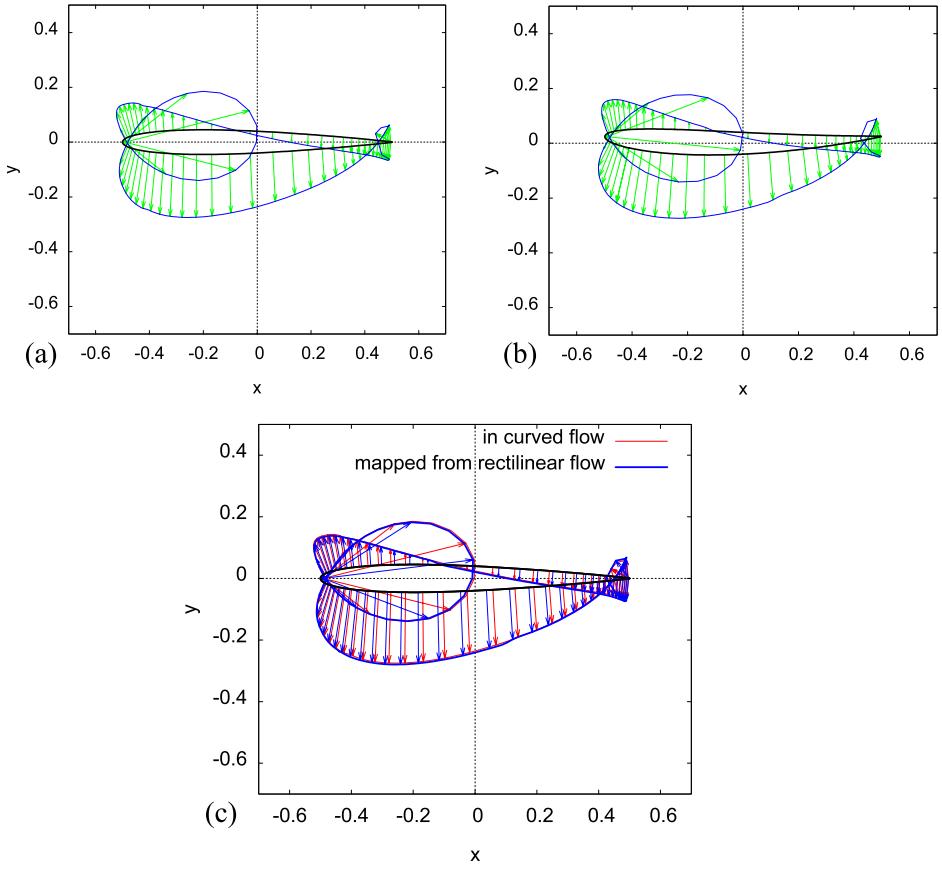

Figure 8. Pressure distributions on NACA0009; (a) in curved flow, (b) modified wing in straight flow and (c) comparison on the distribution on the original geometry ($Re = 3.6 \times 10^6$).

drag does not exist in the theory of ideal flow and the magnitude of drag in the present analysis is small, it may need special treatments.

It should be noted that, in the conventional process of performance prediction, we use the original wing section in the straight flow, neglecting the effect of flow curvature and the resultant lift force. The present analysis indicates that the performance prediction of VAWT should NOT be based on the 2D wind tunnel measurements of the original wing section. For example, lift coefficients of the rotating symmetric wing are over 0.24 without angle of attack, while they will be zero lift in the wind tunnel measurements of the static wing. The authors' recommendation is to use the modified wing section based on the conformal mapping which takes into account the effect of flow curvature. Although the present correlation is based on the theory of ideal fluid, it is applicable to high Reynolds number conditions because of the thin boundary layer. The correlations of viscous effect and stall condition between the curved and straight flows need more discussion.

At present, the effect of incident uniform flow of the turbine has not been considered yet. However, the typical tip speed ratio of VAWT is around 5 and the incident uniform flow is not a dominant component. The treatment of uniform flow will be considered in the future work.

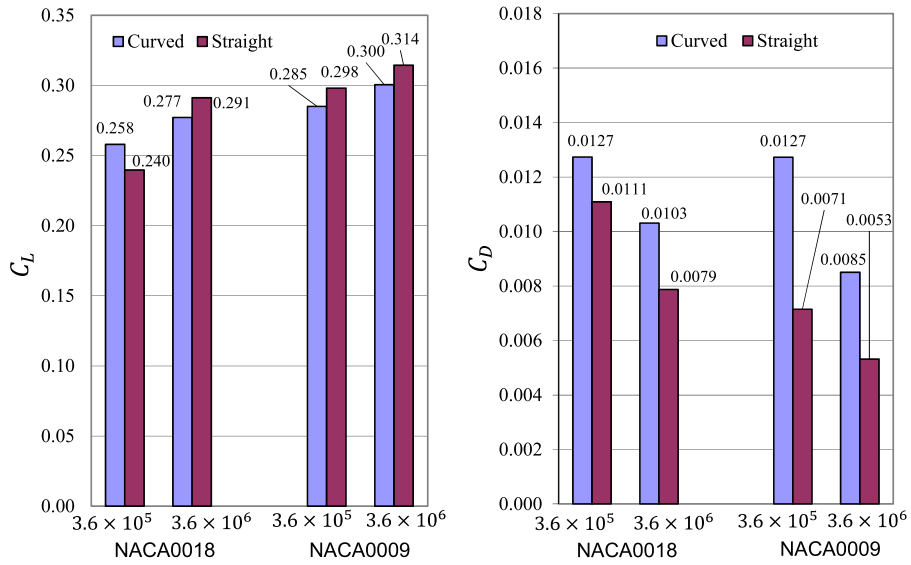

Figure 9. Aerodynamic coefficients of two wing sections in curved flow and their modified sections in the straight flow; (left) lift coefficient and (right) drag coefficient.

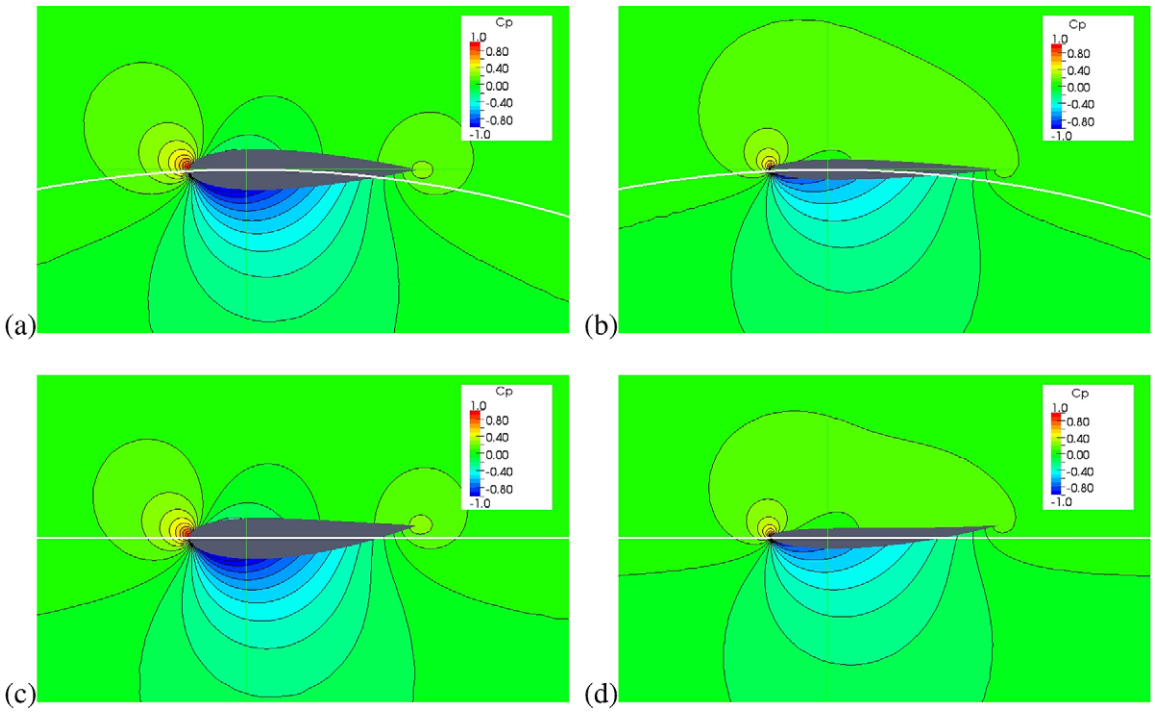

Figure 10. Pressure contour around a wing with reference point 0.25c; (a) NACA0018 in curved flow, (b) NACA0009 in curved flow, (c) mapped NACA0018 in straight flow and (d) mapped NACA0009 in curved flow ($Re = 3.6 \times 10^6$).

3.2. Influence of the reference point of wing

The reference point (mount point) of the wing x_c is shifted from 0.50c to 0.25c to investigate its influence on the flow field. The angle of attack is kept zero at the reference point as shown in figures 10(a) and (b). In comparison to figures 5(a) and 7(a), the increased low pressure on the inner side of wing is obvious.

The resultant aerodynamic coefficients of $x_c = 0.25c$ are shown in figure 11. The lift coefficients are 2.1 times higher than those of $x_c = 0.50c$ conditions in both two wing sections. Although $x_c = 0.25c$ is the aerodynamic center of a typical wing, the zero angle of attack at the point is not the neutral condition because the equivalent wing in the straight flow has an angle of attack as shown in figures 10(c) and (d). It is caused by the fact that, in the curved flow, the distance from the rotating path to the trailing edge is larger than that to the leading edge. It shows that the forward shift of reference point is equivalent to adding the angle of attack.

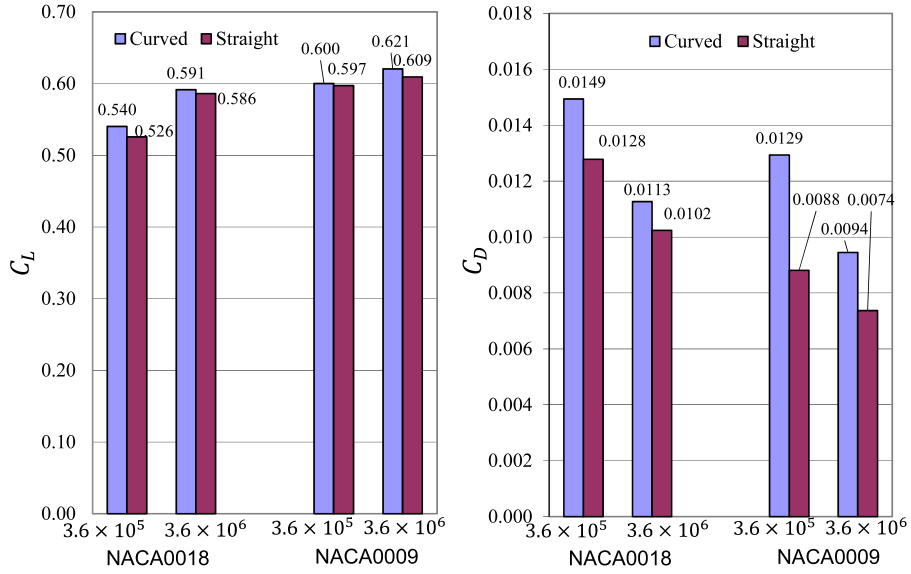

Figure 11. Aerodynamic coefficients of NACA0018 and NACA0009 wing with reference point 0.25c.

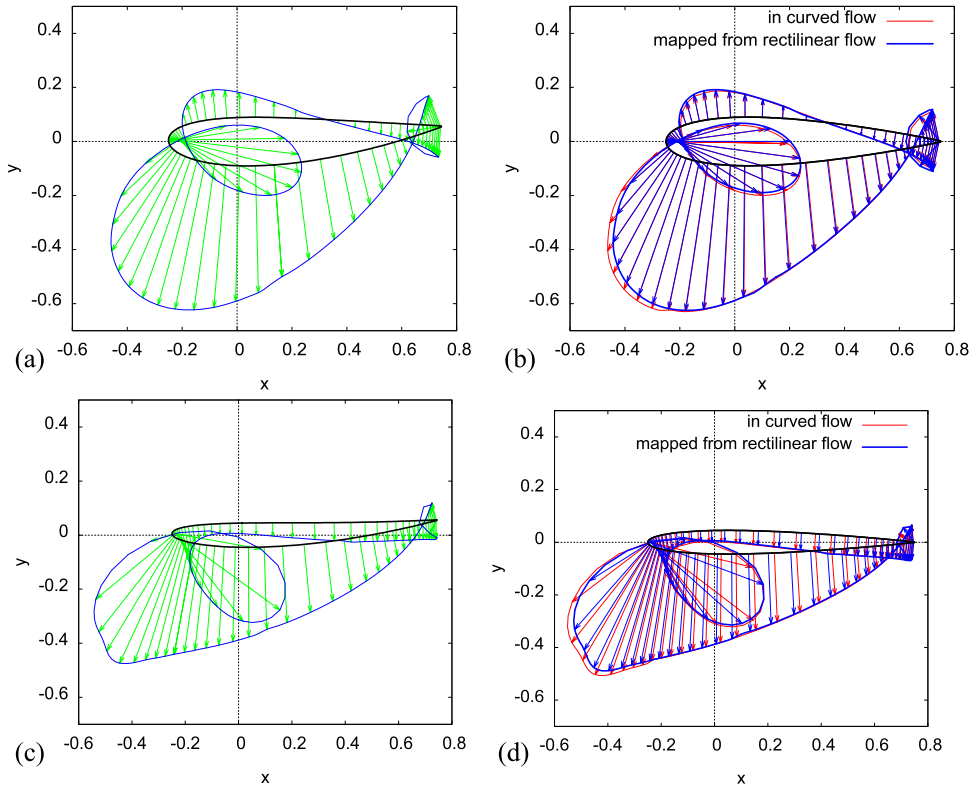

Figure 12. Pressure distribution on two wing sections with reference point 0.25c; (a) mapped NACA0018 in straight flow and (b) comparison on the original wing shape; (c) mapped NACA0009 in straight flow and (d) comparison on the original wing shape ($Re = 3.6 \times 10^6$).

The amount of added attack angle is derived from the mapping function (5) or (6). The leading and trailing edge positions of the mapped wing in the straight flow are $\varsigma_{\mathrm{LE}} = g_2^{-1}(-0.25c)$ and $\varsigma_{\mathrm{TE}} = g_2^{-1}(+0.75c)$ respectively. The effective angle of attack in the straight flow is $\alpha_{\mathrm{eff}} = \arg(\varsigma_{\mathrm{TE}} - \varsigma_{\mathrm{LE}})$. It is 2.827° in the present case (the leading edge is closer to the rotating axis than the trailing edge).

The pressure distributions in the 0.25c reference point cases are shown in figure 12. The pressure distribution on the mapped NACA0018 section is in figure 12(a) and the comparison of remapped and original distributions on the original NACA0018 is in figure 12(b). Those of NACA0009 wing section are shown in figures 12(c) and (d) in the same manner respectively. Although the results show good

agreement between the two conditions, the surface pressure in the straight flow is lower than that of curved flow around the suction peak point near the leading edge. At present, the authors cannot explain the cause of this discrepancy. It is not from the viscous effect because the boundary layer is thin there and the authors observed the similar magnitude of discrepancy also in the low Reynolds number cases.

The result indicates that description of the reference point is indispensable along with the setting attack angle to determine the effective attack angle of the rotating blade. However, in much of the researches for VAWT, the information of reference point is missing. It makes the comparisons of VAWTs difficult and sometimes conclusions are not consistent among research groups. The incompleteness of setting information should be resolved for the further development of VAWT. The proposed method of conformal mapping is effective for understanding the condition of rotating blade subjected to curved ambient flow.

4. Conclusion

The authors proposed a complex variable conformal mapping method between the curved flow around a rotating turbine blade and the straight flow around a modified wing. The proposed regular function keeps the ideal flow condition in the bidirectional mapping. The results showed that the influence of flow curvature can be replaced by the effect of additional camber of the mapped wing. The mechanism of virtual camber is mathematically defined. The proposed method leads to the effective utilization of 2D static wing measurements and 2D RaNS simulations that are less expensive than the analysis of rotating turbine. It will be beneficial to the R&D of VAWT which is increasingly important for the floating offshore wind turbine. Naturally, the method is also applicable to the vertical axis marine current turbine.

The analysis also explains the significant influence of the reference point position (mount point of the blade) on the flow field. The forward shift of reference point increases the effective attack angle of the blade. The condition is well understood in the straight flow field around the equivalent wing section generated by the proposed conformal mapping.

In the previous research for VAWTs, the development of the blade shape has often been effectively by trial and error. However, with the present mapping method, we can utilize the accumulated knowledge of 2D wing sections in VAWT. The geometry of a blade can be described as in the usual theory of wing sections in the mapped straight flow. Since the present analysis does not include the incident uniform wind for simplicity, it requires further extension. Also, validation of the present approach in the performance prediction of practical turbine should be provided in the future work.

Acknowledgment

This research was supported by WCU (World Class University) program through the National Research Foundation of Korea funded by the Ministry of Education, Science and Technology (R31-2008-000-10045-0).

References

[1] Muraca R J, Stephens M V and Dagenhart J R 1975 *Theoretical Performance of Cross-Wind Axis Turbines With Results for a Catenary Vertical Axis Configuration* NASA-TM-X-72662, NASA, Langley Research Center

[2] Milgliore P G and Wolfe W P 1979 Some effects of flow curvature on the performance of Darrieus wind turbines *17th Aerospace Sciences Mtg. AIAA 79-0112*

[3] Migliore P G, Wolfe W P and Fanucci J B 1980 Flow curvature effects on Darrieus turbine blade aerodynamics *J. Energy* **4** 49–55

[4] Migliore P G and Wolfe W P 1980 Some effects of flow curvature on the aerodynamics of Darrieus wind turbine *Report Prepared for DOE Under Contract* EY-76-C-05-5135 West Virginia University

[5] Strickland J H 1975 A performance prediction model using multiple streamtubes *Tech. Report* Sandia National Labatories

[6] Paraschivoiu I 1981 Double-multiple streamtube model for Darrieus wind turbines *2nd DOE/NASA Wind Turbines Dynamics Workshop, NASA CP-2186 (OH)* pp 19–25

[7] Abbott I H and Von Doenhoff A E 1959 *Theory of Wing Sections: Including a Summary of Airfoil Data* (New York: Dover Books on Physics)

[8] Sheldahl R E and Klimas P C 1981 *Aerodynamic Characteristics of Seven Symmetrical Airfoil Sections Through 180-degree Angle of Attack for Use in Aerodynamic Analysis of Vertical Axis Wind Turbines* No. SAND-80-2114 (Albuquerque, NM: Sandia National Labs)

[9] Paulsen U S *et al* 2011 Deepwind—an innovative wind turbine concept for offshore *Proc. EWEA Annual Event 2011 (Brussels)* p 9

[10] Akimoto H, Tanaka K and Uzawa K 2011 Floating axis wind turbines for offshore power generation—a conceptual study *Environ. Res. Lett.* **6** 044017

[11] Collu M, Brennan F P and Patel M H 2012 Conceptual design of a floating support structure for an offshore vertical axis wind turbine: the lessons learnt *Ships Offshore Struct.* 1–19

[12] Nakamura T, Mizumukai K, Akimoto H, Hara Y and Kawamura T 2013 Floating axis wind and water turbine for high utilization of sea surface area (design of sub-megawatt prototype turbine) *Proc. OMAE2013, OMAE2013-11287 (Nantes)*

[13] Akimoto H, Tanaka K and Uzawa K 2013 A conceptual study of floating axis water current turbine for low-cost energy capturing from river, tide and ocean currents *Renew. Energy* **57** 283–8

[14] Akimoto H, Tanaka K, Hara Y and Uzawa K 2013 Design and estimated economic performance of a floating axis marine current turbine in Kuroshio ocean current *Proc. OMAE2013, OMAE2013-10828 (Nantes)*

[15] Ågren O, Berg M and Leijon M 2005 A time-dependent potential flow theory for the aerodynamics of vertical axis wind turbines *J. Appl. Phys.* **97** 104913

[16] Furukawa A, Takamatsu Y and Takenouchi K 1990 *Theoretical Considerations in an Approximate Method for Estimating the Blade Performance of a Darrieus-type Cross-Flow Water Turbine* vol 50 Memoirs of the Faculty of Engineering, Kyushu University pp 1–14

[17] Takamatsu Y, Furukawa A, Takenouchi K and Okuma K 1993 Experimental considerations in an approximate method for estimating the blade performance of Darrieus-type cross-flow water turbines *JSME Int. J.* B **36** 135–42